

Block modelling in dynamic networks with non homogeneous Poisson processes and exact ICL

Marco Corneli^a, Pierre Latouche^a, Fabrice Rossi^a

^a*Université Paris 1 Panthéon-Sorbonne - Laboratoire SAMM
90 rue de Tolbiac, F-75634 Paris Cedex 13 - France*

Abstract

We develop a model in which interactions between nodes of a dynamic network are counted by non homogeneous Poisson processes. In a block modelling perspective, nodes belong to hidden clusters (whose number is unknown) and the intensity functions of the counting processes only depend on the clusters of nodes. In order to make inference tractable we move to discrete time by partitioning the entire time horizon in which interactions are observed in fixed-length time sub-intervals. First, we derive an exact integrated classification likelihood criterion and maximize it relying on a greedy search approach. This allows to estimate the memberships to clusters and the number of clusters simultaneously. Then a maximum-likelihood estimator is developed to estimate non parametrically the integrated intensities. We discuss the over-fitting problems of the model and propose a regularized version solving these issues. Experiments on real and simulated data are carried out in order to assess the proposed methodology.

Keywords: Dynamic network, Stochastic block model, exact ICL, Non homogeneous Poisson Process.

1. Introduction

Graph clustering (Schaeffer, 2007) is probably one of the main exploratory tools used in network analysis as it provides data analysts with a high level summarized view of complex networks. One of the main paradigms for graph clustering is community search (Fortunato, 2010): a *community* is a subset of nodes in a graph that are densely connected and have relatively few connections to nodes outside of the community. While this paradigm is very successful in many applications, it suffers from a main limitation: it cannot be used to detect other important structures that arise in graphs, such as bipartite structures, hubs, authorities, and other patterns.

The alternative solution favoured in this paper is provided by block models (Lorrain and White, 1971; White et al., 1976): in such a model, a cluster consists of nodes that share the same connectivity patterns to other clusters, regardless of the pattern itself (community, hub, bipartite, etc.). A popular probabilistic view on block models is provided by the stochastic block model (SBM, Holland et al.,

1983; Wang and Wong, 1987). The main idea is to assume that a hidden random variable is attached to each node. This variable contains the cluster membership information while connection probabilities between clusters are handled by the parameters of the model. The reader is sent to Goldenberg et al. (2009) for a survey of probabilistic models for graphs and to Wasserman and Faust (1994),
20 Ch.16, for an overview of the stochastic block models

This paper focuses on dynamic graphs in the following sense: we assume that nodes of the graph are fixed and that interactions between them are directed and take place at a specific instant. In other words, we consider a directed
25 multi-graph (two nodes can be connected by more than one edge) in which each directed edge is labelled with an occurrence time. We are interested in extending the SBM to this type of graphs. More precisely, the proposed model is based on a counting process point of view of the interactions between nodes: we assume that the number of interactions between two nodes follows a non homogeneous
30 Poisson counting process (NHPP). As in a standard SBM, nodes are assumed to belong to clusters that do not change over time, thus the temporal aspect is handled only via the non homogeneity of the counting processes. Then the block model hypothesis take the following form: the intensity of the NHPP that counts interactions between two nodes depends only on the clusters of the nodes. In
35 order to obtain a tractable inference, a segmentation of the time interval under study is introduced and the interactions are aggregated over the sub-intervals of the partition. Following Côme and Latouche (2015), the model is adjusted to the data via the maximization of the integrated classification likelihood (ICL Biernacki et al., 2000) in an exact form. As in Côme and Latouche (2015) (and
40 Wyse et al. (2014) for latent block models), the maximization is done via a greedy search. This allows us to chose automatically the number of clusters in the block model.

When the number of sub-intervals is large, the model can suffer from a form of over fitting as the ICL penalizes only a large number of clusters. Therefore,
45 we introduce a variant, based on the model developed in Corneli et al. (2015), in which sub-intervals are clustered into classes of homogeneous intensities. Those clusters are accounted for in a new version of the ICL which prevents over fitting.

This paper is structured as follows: in Section 2 we mention works related to the approach we propose, Section 3 presents the proposed temporal extension of the SBM, Section 4 derives the exact ICL for this model and presents the greedy
50 search algorithm used to maximize the ICL. Section 5 gathers experimental results on simulated data and on real world data. Section 6 concludes the paper.

2. Related Works

Numerous extensions of the original SBM have already been proposed to deal
55 with dynamic graphs. In this context, both nodes memberships to a cluster and interactions between nodes can be seen as stochastic processes. In Yang et al. (2011), for instance, authors introduce a Markov Chain to obtain the cluster of node in t given its cluster at time $t - 1$. Xu and Hero III (2013) as well as Xing et al. (2010) used a state space model to describe temporal changes at

60 the level of the connectivity pattern. In the latter, the authors developed a method to retrieve overlapping clusters through time. In general, the proposed temporal variations of the SBM share a similar approach: the data set consists in a sequence of graphs rather than the more general structure we assume. Some papers remove those assumptions by considering continuous time models in which
65 edges occur at specific instants (for instance when someone sends an email). This is the case of e.g. Dubois et al. (2013) and of Guigourès et al. (2012, 2015). A temporal stochastic block model, related to the one presented in this paper is independently developed by Matias et al. (2015). They assume that nodes in a network belong to clusters whose composition do not change over time and
70 interactions are counted by a non-homogeneous Poisson process whose intensity only depends on the nodes clusters. In order to estimate (non-parametrically) the instantaneous intensity functions of the Poisson processes, they develop a variational EM algorithm to maximize an approximation of the likelihood.

3. The model

75 We consider a fixed set of N nodes, $\{1, \dots, N\}$, that can interact as frequently as wanted during the time interval $[0, T]$. Interactions are directed from one node to another and are assumed to be instantaneous¹. A natural mathematical model for this type of interactions is provided by counting processes on $[0, T]$. Indeed a counting process is a stochastic process with values that are non negative
80 integers increasing through time: the value at time t can be seen as the number of interactions that took place from 0 to t . Then the classical adjacency matrix $(X_{ij})_{1 \leq i, j \leq N}$ of static graphs is replaced by a $N \times N$ collection of counting processes, $(X_{ij}(t))_{1 \leq i, j \leq N}$, where $X_{ij}(t)$ is the counting process that gives the number of interactions from node i to node j . We still call $\mathbf{X} = (X_{ij}(t))_{1 \leq i, j \leq N}$
85 the adjacency matrix of this dynamical graph.

We introduce in this Section a generative model for adjacency matrices of dynamical graphs that is inspired by the classical stochastic block model (SBM).

3.1. Non-homogeneous Poisson counting process

We first chose a simple form for $X_{ij}(t)$: we assume that this process is a non-homogeneous Poisson counting process (NHPP) with instantaneous intensity given by the function from $[0, T]$ to \mathbb{R} , λ_{ij} . For $s \leq t \leq T$, it then holds

$$p(X_{ij}(t) - X_{ij}(s) | \lambda_{ij}) = \frac{(\int_s^t \lambda_{ij}(u) du)^{X_{ij}(t) - X_{ij}(s)}}{(X_{ij}(t) - X_{ij}(s))!} \exp\left(-\int_s^t \lambda_{ij}(u) du\right), \quad (1)$$

where $X_{ij}(t) - X_{ij}(s)$ is the (non negative) number of interactions from i to j
90 that took place during $[s, t]$. (We assume that $X_{ij}(0) = 0$.)

¹In practice, the starting time of an interaction with a duration will be considered.

3.2. Block modelling

The main idea of the SBM (Holland et al., 1983; Wang and Wong, 1987) is to assume that nodes have some (hidden) characteristics that solely explain their interactions, in a stochastic sense. In our context this means that rather than
 95 having pairwise intensity functions λ_{ij} , those functions are shared by nodes that have the same characteristics.

In more technical terms, we assume the nodes are grouped in K clusters $(\mathcal{A}_1, \dots, \mathcal{A}_K)$ and introduce a hidden cluster membership random vector $\mathbf{z} \in \{1, \dots, K\}^N$ such that

$$z_i = k \quad \text{iff} \quad i \in \mathcal{A}_k, \quad k \leq K.$$

The random component z_i is assumed to follow a multinomial distribution with parameter vector ω such that

$$\mathbb{P}\{z_i = k\} = \omega_k \quad \text{with} \quad \sum_{k \leq K} \omega_k = 1.$$

In addition, the $(z_i)_{1 \leq i \leq N}$ are assumed to be independent (knowing ω) and thus

$$p(\mathbf{z}|\omega, K) = \prod_{k \leq K} \omega_k^{|\mathcal{A}_k|}, \quad (2)$$

where $|\mathcal{A}_k|$ denotes the cardinal of \mathcal{A}_k . Notice that this part of the model is exactly identical to what is done in the classical SBM.

In a second step, we assume that given \mathbf{z} , the counting processes $X_{ij}(t)$ are
 100 independent and in addition that the intensity function λ_{ij} depends only on z_i and z_j . In order to keep notations tight we denote $\lambda_{z_i z_j}$ the common intensity function and we will not use directly the pairwise intensity functions λ_{ij} . We denote $\boldsymbol{\lambda}$ the matrix valued intensity function $\boldsymbol{\lambda} = (\lambda_{kg}(t))_{1 \leq k, g \leq K}$.

Combining all the assumptions, we have for $s \leq t \leq T$

$$p(\mathbf{X}(t) - \mathbf{X}(s) | \mathbf{z}, \boldsymbol{\lambda}) = \prod_{i \neq j} \frac{(\int_s^t \lambda_{z_i z_j}(u) du)^{X_{ij}(t) - X_{ij}(s)}}{(X_{ij}(t) - X_{ij}(s))!} \exp\left(-\int_s^t \lambda_{z_i z_j}(u) du\right). \quad (3)$$

3.3. Discrete time version

In order to make inference tractable, we move from the continuous time model to a discrete time one. This is done via a partition of the interval $[0, T]$ based on a set of $U + 1$ instants

$$0 = t_0 \leq t_1 \leq \dots \leq t_{U-1} \leq t_U = T,$$

that defines U intervals $I_u := [t_{u-1}, t_u[$ (with arbitrary length Δ_u). The purpose of the partition is to aggregate the interaction. Let us denote

$$Y_{ij}^{I_u} := X_{ij}(t_u) - X_{ij}(t_{u-1}), \quad u \in \{1, \dots, U\}. \quad (4)$$

In words, $Y_{ij}^{I_u}$ measures the increment, over the time interval I_u , of the Poisson process counting interactions from i to j . We denote by Y_{ij} the random vector

$$Y_{ij} := (Y_{ij}^{I_1}, \dots, Y_{ij}^{I_U})^T.$$

Thanks to the independence of the increments of a Poisson process, we get the following joint density:

$$p(Y_{ij}|\lambda_{ij}) = \prod_{u=1}^U \left(\frac{(\int_{I_u} \lambda_{ij}(s) ds)^{Y_{ij}^{I_u}}}{Y_{ij}^{I_u}!} \exp\left(-\int_{I_u} \lambda_{ij}(s) ds\right) \right). \quad (5)$$

The variations of λ_{ij} inside an interval I_u have no effect on the distribution of Y_{ij} . This allows us to use the integrated intensity function Λ defined on $[0, T]$ by

$$\Lambda_{ij}(t) := \int_0^t \lambda_{ij}(s) ds.$$

In addition, we denote by $\pi_{ij}^{I_u}$ the increment of the integrated intensity function over I_u

$$\pi_{ij}^{I_u} := \Lambda_{ij}(t_u) - \Lambda_{ij}(t_{u-1}), \quad \forall u \in \{1, \dots, U\}.$$

Then equation (5) becomes

$$p(Y_{ij}|\pi_{ij}) = \prod_{u=1}^U \left(\frac{(\pi_{ij}^{I_u})^{Y_{ij}^{I_u}}}{Y_{ij}^{I_u}!} \exp\left(-\pi_{ij}^{I_u}\right) \right), \quad (6)$$

105 with $\pi_{ij} := (\pi_{ij}^{I_1}, \dots, \pi_{ij}^{I_U})^T$.

Using the block model assumptions, we have in addition

$$p(Y_{ij}|\pi_{z_i z_j}, z_i, z_j) = \prod_{u=1}^U \left(\frac{(\pi_{z_i z_j}^{I_u})^{Y_{ij}^{I_u}}}{Y_{ij}^{I_u}!} \exp\left(-\pi_{z_i z_j}^{I_u}\right) \right), \quad (7)$$

where we have used the fact that $\lambda_{ij} = \lambda_{z_i z_j}$ (which leads to $\Lambda_{ij} = \Lambda_{z_i z_j}$, etc.).

110 Considering the network as a whole, we can introduce two tensors of order 3. Y is a $N \times N \times U$ random tensor whose element (i, j, u) is the random variable $Y_{ij}^{I_u}$ and π is the $K \times K \times U$ tensor whose element (k, g, u) is $\pi_{kg}^{I_u}$. Y can be seen as an aggregated (or discrete time version) of the adjacency process \mathbf{X} while π can be seen as summary of the matrix valued intensity function $\boldsymbol{\lambda}$.

The conditional independence assumption of the block model leads to

$$p(Y|\pi, \mathbf{z}) = \prod_{i,j}^N p(Y_{ij}|\pi_{z_i z_j}, z_i, z_j). \quad (8)$$

To simplify the rest of the paper, we will use the following notations

$$\prod_{i,j} \prod_{k,g} \prod_u := \prod_{i=1}^N \prod_{j=1}^N \prod_{k=1}^K \prod_{g=1}^K \prod_{u=1}^U$$

$$\prod_{z_i=k} \left(\prod_{z_j=g} \right) := \prod_{\substack{i: \\ z_i=k}} \left(\prod_{\substack{j: \\ z_j=g}} \right).$$

The joint distribution of Y , given \mathbf{z} and π , is

$$\begin{aligned} p(Y|\mathbf{z}, \pi) &= \prod_{i,j} \prod_u \left(\frac{(\pi_{z_i z_j}^{I_u})^{Y_{ij}^{I_u}}}{Y_{ij}^{I_u}!} \exp(-\pi_{z_i z_j}^{I_u}) \right) \\ &= \prod_{k,g} \prod_u \left(\frac{(\pi_{k,g}^{I_u})^{S_{kgu}}}{P_{kgu}} \exp(-|A_k| |A_g| \pi_{kg}^{I_u}) \right), \end{aligned} \quad (9)$$

where

$$S_{kgu} = \sum_{z_i=k} \sum_{z_j=g} Y_{ij}^{I_u},$$

is the total number of interactions from cluster k to cluster g (possibly equal to k) and with

$$P_{kgu} = \prod_{z_i=k} \prod_{z_j=g} Y_{ij}^{I_u}!.$$

3.4. A constrained version

As will be shown in Section 4.4, the model presented thus far is prone to over fitting when the number of sub-intervals U is large compared to N . Additional constraints on the intensity functions $\{\Lambda_{kg}(t)\}_{k,g \leq K}$ are needed in this situation.

Let us consider a fixed pair of clusters (k, g) . So far, the increments $\{\pi_{kg}^{I_u}\}_{u \leq U}$ are allowed to differ on each I_u over the considered partition. A constraint can be introduced by assigning the time intervals (I_1, \dots, I_U) to different time clusters and assuming that increments are identical for all the intervals belonging to the same time cluster. Formally, we introduce D clusters $(\mathcal{C}_1, \dots, \mathcal{C}_D)$ and a hidden random vector $\mathbf{y} \in \{0, 1\}^U$, labelling memberships

$$y_u = d \quad \text{iff} \quad I_u \in \mathcal{C}_d.$$

Each y_u is assumed to follow a multinomial distribution depending on parameter $\boldsymbol{\rho}$

$$\mathbb{P}\{y_u = d\} = \rho_d \quad \text{with} \quad \sum_{d \leq D} \rho_d = 1,$$

and in addition the y_u are assumed to be independent, leading to

$$p(\mathbf{y}|\boldsymbol{\rho}, D) = \prod_{d \leq D} \rho_d^{|\mathcal{C}_d|}. \quad (10)$$

The random variable $Y_{ij}^{I_u}$ is now assumed to follow the conditional distribution

$$p(Y_{ij}^{I_u} | \mathbf{z}, \mathbf{y}) = \frac{(\pi_{z_i z_j}^{y_u})^{Y_{ij}^{I_u}}}{Y_{ij}^{I_u}!} \exp(-\pi_{z_i z_j}^{y_u}). \quad (11)$$

Notice that the new Poisson parameter $\pi_{z_i z_j}^{y_u}$ replaces $\pi_{z_i z_j}^{I_u}$ in the unconstrained version. The joint distribution of Y , given \mathbf{z} and \mathbf{y} , can easily be obtained

$$p(Y | \mathbf{z}, \mathbf{y}, \pi) = \prod_{k,g} \prod_d \left(\frac{(\pi_{kg}^d)^{S_{kgd}}}{P_{kgd}} \exp(-|\mathcal{A}_k| |\mathcal{A}_g| |\mathcal{C}_d| \pi_{kg}^d) \right), \quad (12)$$

where

$$S_{kgd} = \sum_{z_i=k} \sum_{z_j=g} \sum_{y_u=d} Y_{ij}^{I_u}, \quad P_{kgd} = \prod_{z_i=k} \prod_{z_j=g} \prod_{y_u=d} Y_{ij}^{I_u}!$$

Remark 1. *The introduction of this hidden vector \mathbf{y} is not the only way to impose regularity constraints to the integrated function $\Lambda_{kg}(t)$. For example, a segmentation constraint could be imposed by forcing each temporal cluster to contain only adjacent time intervals.*

120 3.4.1. Summary

We have defined two generative models:

Model A the model has two meta parameters, K the number of clusters and $\boldsymbol{\omega}$ the parameters of a multinomial distribution on $\{1, \dots, K\}$. The hidden variable \mathbf{z} is generated by the multivariate multinomial distribution of equation (2). Then the model has a $K \times K \times U$ tensor of parameters π . Given \mathbf{z} and π , the model generates a tensor of interaction counts Y using equation (9). 125

Model B is a constrained version of model **A**. In addition to the meta parameters K and $\boldsymbol{\omega}$ of model **A**, it has two meta parameters, D the number of clusters of time sub-intervals and $\boldsymbol{\rho}$ the parameters of a multinomial distribution on $\{1, \dots, D\}$. The hidden variable \mathbf{y} is generated by the multivariate multinomial distribution of equation (10). Model **B** has a $K \times K \times D$ tensor of parameters π . Given \mathbf{z} , \mathbf{y} and π , the model generates a tensor of interaction counts Y using equation (12). 130

135 Unless specified otherwise “the model” is used for model **A**.

4. Estimation

4.1. Non parametric estimation of integrated intensities

In this Section we assume that \mathbf{z} is known. No hypothesis has been formulated about the shape of the functions $\{\Lambda_{kg}(t)\}_{\{k,g \leq K, t \leq T\}}$ and the increments of these

functions over the partition introduced can be estimated by maximum likelihood (ML), thanks to equation (9)

$$\log \mathcal{L}(\pi|Y, \mathbf{z}) = \sum_{k,g} \sum_u \left[S_{kgu} \log(\pi_{kg}^{I_u}) - |\mathcal{A}_k| |\mathcal{A}_g| \pi_{kg}^{I_u} + c \right],$$

where c denotes those terms not depending on π . It immediately follows

$$\hat{\pi}_{kg}^{I_u} = \frac{S_{kgu}}{|\mathcal{A}_k| |\mathcal{A}_g|}, \quad \forall (k, g), \quad (13)$$

where $\hat{\pi}_{kg}^{I_u}$ denotes the ML estimator of $\pi_{kg}^{I_u}$. In words, $\Lambda_{kg}(t_u) - \Lambda_{kg}(t_{u-1})$ can be estimated by ML as the total number of interactions on the sub-graph corresponding to the connections from cluster A_k to cluster A_g , over the time interval I_u , divided by the number of nodes on this sub-graph. Once the tensor π has been estimated, we have a point-wise, non parametric estimator of $\Lambda_{kg}(t_u)$, for every $u \leq U$, defined by

$$\hat{\Lambda}_{kg}(t_u) = \sum_{l=1}^u \hat{\pi}_{kg}^{I_l}, \quad \forall (k, g). \quad (14)$$

Thanks to the properties of the ML estimator, together with the linearity of (14), we know that $\hat{\Lambda}_{kg}(t_u)$ is an unbiased and convergent estimator of $\Lambda_{kg}(t_u)$.

140 **Remark 2.** *Estimator (14) at times $\{t_u\}_{u \leq U}$, can be viewed as an extension to random graphs and mixture models of the non parametric estimator proposed in Leemis (1991). In that article, N -trajectories of independent NHPPs, sharing the same intensity function, are observed and the proposed estimator is basically obtained via method of moments.*

In all the experiments, we consider the following step-wise linear estimator of $\Lambda_{kg}(t)$

$$\hat{\Lambda}_{kg}(t) = \sum_{u=1}^U \left[\hat{\Lambda}_{kg}(t_{u-1}) + \frac{\hat{\Lambda}_{kg}(t_u) - \hat{\Lambda}_{kg}(t_{u-1})}{t_u - t_{u-1}} (t - t_{u-1}) \right] \mathbf{1}_{[t_{u-1}, t_u[}(t), \quad (15)$$

145 which is a linear combination of estimators in equation (14) on the interval $[0, T]$. This is a consistent and unbiased estimator of $\Lambda_{kg}(t)$ at times $\{t_u\}_{u \leq U}$ only.

When considering model **B**, equations (13) and (14) are replaced by

$$\hat{\pi}_{kg}^d = \frac{S_{kgd}}{|\mathcal{A}_k| |\mathcal{A}_g| |\mathcal{C}_d|} \quad (16)$$

$$\hat{\Lambda}_{kg}(t_u) = \sum_{l=1}^u \hat{\pi}_{kg}^{y_l}. \quad (17)$$

Equation (15) remains unchanged, but an important difference between the constrained model and the unconstrained one should be understood: in the former, each interval I_u corresponds to a different slope for the function $\hat{\Lambda}_{kg}(t)$ whereas in the latter we only have D different slopes, one for each time cluster.

150

4.2. ICL

Since the vector \mathbf{z} , as well as the number of clusters K are unknown, estimator (13) cannot be used directly. Hence we propose a two step procedure consisting in

- 155 1. providing estimates of \mathbf{z} and K ,
2. using these estimates to implement (13) and (14).

To accomplish the first task, the same approach followed in Côme and Latouche (2015) is adopted: we directly maximize the the joint integrated log-likelihood of complete data (ICL), relying on a greedy search over the labels and number of clusters. To perform such a maximization, we need the ICL to have an explicit form. This can be achieved by introducing conjugated prior distributions on the model parameters. The ICL can be written as

$$\mathcal{ICL}(\mathbf{z}, K) := \log(p(Y, \mathbf{z}|K)) = \log(p(Y|\mathbf{z}, K)) + \log(p(\mathbf{z}|K)). \quad (18)$$

This *exact* quantity is approximated by the well known ICL *criterion* (Biernacki et al., 2000). This criterion, obtained through Laplace and Stirling approximations of the joint density on the left hand side of equation (18), is used as a
 160 model selection tool, since it penalizes models with a high number of parameters. In the following, we refer to the joint log-density in equation (18) as to the *exact ICL* to differentiate it from the ICL criterion.

We are now going to study in detail the two quantities on the r.h.s. of the above equation. The first probability density is obtained by integrating out the parameter π

$$p(Y|\mathbf{z}, K) = \int p(Y, \pi|\mathbf{z}, K)d\pi.$$

In order to have an explicit formula for this term, we impose the following Gamma prior conjugated density over the tensor π :

$$p(\pi|a, b) = \prod_{k,g,u} \frac{b^a}{\Gamma(a)} \pi_{kgu}^{a-1} e^{-b\pi_{kgu}},$$

where the hyper-parameters of the Gamma prior distribution have been set constant to a and b for simplicity.² By using the Bayes rule

$$p(Y, \pi|\mathbf{z}) = p(Y|\pi, \mathbf{z})p(\pi|a, b),$$

we get:

$$p(Y, \pi|\mathbf{z}) = \prod_{k,g,u} \frac{b^a}{\Gamma(a)P_{kgu}} \pi_{kgu}^{S_{kgu}+a-1} \times \exp(-\pi_{kgu} [|\mathcal{A}_k||\mathcal{A}_g| + b]),$$

²The model can easily be extended to the more general framework:

$$p(\pi_{kgu}|a_{kgu}, b_{kgu}) = \text{Gamma}(\pi_{kgu}|a_{kgu}, b_{kgu}).$$

which can be integrated with respect to π to obtain

$$p(Y|\mathbf{z}, K) = \prod_{k,g,u} \left[\frac{b^a}{\Gamma(a)P_{kgu}} \frac{\Gamma[S_{kgu} + a]}{[|\mathcal{A}_k||\mathcal{A}_g| + b]^{(S_{kgu} + a)}} \right]. \quad (19)$$

We now focus on the second density on the right hand side

$$p(\mathbf{z}|K) = \int p(\mathbf{z}, \boldsymbol{\omega}|K) d\boldsymbol{\omega}.$$

A Dirichlet *prior* distribution can be attached to $\boldsymbol{\omega}$ in order to get an explicit formula, in a similar fashion of what we did with π :

$$\nu(\boldsymbol{\omega}|K) = \text{Dir}_K(\boldsymbol{\omega}; \alpha, \dots, \alpha).$$

The integrated density $p(\mathbf{z}|K)$ can be proven to reduce to

$$p(\mathbf{z}|K) = \frac{\Gamma(\alpha K)}{\Gamma(\alpha)^K} \frac{\prod_{k \leq K} \Gamma(|\mathcal{A}_k| + \alpha)}{\Gamma(N + \alpha K)} \quad (20)$$

4.3. Model B

When considering the constrained framework described at the end of the previous section, the ICL is defined

$$\begin{aligned} \mathcal{ICL}(\mathbf{z}, \mathbf{y}, K, D) &:= \log(p(Y, \mathbf{z}, \mathbf{y}|K, D)) \\ &= \log(p(Y|\mathbf{z}, \mathbf{y})) + \log(p(\mathbf{z}|K)) + \log(p(\mathbf{y}|D)) \end{aligned}$$

and it is maximized to provide estimates of \mathbf{z} , \mathbf{y} , K and D . The first density on the right hand side is obtained by integrating out the hyper-parameter π . This integration can be done explicitly by attaching to π the following prior density function

$$\nu(\pi|a, b) = \prod_{k,g} \prod_d \frac{b^a}{\Gamma(a)} \pi_{kgd}^{a-1} e^{-b\pi_{kgd}}.$$

The second integrated density on the right hand side can be read in (20) and the third is obtained by integrating out the parameter $\boldsymbol{\rho}$, whose prior density function is assumed to be

$$\nu(\boldsymbol{\rho}|D) = \text{Dir}_D(\boldsymbol{\rho}; \beta, \dots, \beta).$$

The exact ICL is finally obtained by taking the logarithm of

$$\begin{aligned} p(Y, \mathbf{z}, \mathbf{y}|K, D) &= \prod_{k,g,d} \frac{b^a}{\Gamma(a)P_{kgd}} \frac{\Gamma[S_{kgd} + a]}{[|\mathcal{A}_k||\mathcal{A}_g||\mathcal{C}_d| + b]^{(S_{kgd} + a)}} \\ &\times \frac{\Gamma(\alpha K)}{\Gamma(\alpha)^K} \frac{\prod_{k \leq K} \Gamma(|\mathcal{A}_k| + \alpha)}{\Gamma(N + \alpha K)} \\ &\times \frac{\Gamma(\beta D)}{\Gamma(\beta)^D} \frac{\prod_{d \leq D} \Gamma(|\mathcal{C}_d| + \beta)}{\Gamma(U + \beta D)}. \end{aligned} \quad (21)$$

4.4. Greedy search

By setting conjugated prior distributions over the model parameters, we obtained an ICL (equation (18)) in an explicit form. Nonetheless explicit formulas to maximize it, with respect to \mathbf{z} and K , do not exist. We then rely on a greedy search algorithm, that has been used to maximize the exact ICL, in the context of a standard SBM, by Côme and Latouche (2015). This algorithm basically works as follows:

1. An initial configuration for both \mathbf{z} and K is set (standard clustering algorithms like *k-means* or hierarchical clustering can be used).
2. Labels switches leading to the highest increase in the exact ICL are repeatedly made. A label switch consists in a merge of two clusters or in a node switch from one cluster to another.

Remark 3. *The greedy algorithm described in this section, makes the best choice locally. A convergence toward the global optimum is not guaranteed and often this optimum can only be approximated by a local optimum reached by the algorithm.*

Remark 4. *The exact ICL (as well as the ICL criterion) penalizes the number of parameters. Since the tensor π has dimension $K \times K \times U$, when U , which is fixed, is very high, the ICL will take its maximum for $K = 1$. In other words the only way the ICL has to make the model more parsimonious is to reduce K up to one. By doing so, any community (or other) structure will not be detected. This over-fitting problem has nothing to see with the possible limitations of the greedy search algorithm and it can be solved by switching to model \mathcal{B} .*

Once K_{max} has been fixed, together with an initial value of \mathbf{z} , a shuffled sequence of all the nodes in the graph is created. Each node in the sequence is moved to the cluster leading to the highest increase in the ICL, if any. This procedure is repeated until no further increase in the ICL is still possible. Henceforth, we refer to this step as to *Greedy-Exchange (GE)*. When maximizing the modularity score to detect communities, the **GE** usually is a final refinement step to be adopted after repeatedly merging clusters of nodes. In that context, moreover, the number of clusters is initialized to U and each node is alone in its own cluster. See for example Noack and Rotta (2008). Here, we follow a different approach, proposed by Côme and Latouche (2015) and Blondel et al. (2008): after running the GE, we try to *merge* the remaining clusters of nodes in the attempt to increase the ICL. In this final step (henceforth **GM**), all the possible merges are tested and the best one is retained.

The ICL does not have to be computed before and after each swap/merge: possible increases can be assessed directly. When switching one node (say i) from cluster $\mathcal{A}_{k'}$ to \mathcal{A}_l , with $k' \neq l$, the change in the ICL is given by³

$$\Delta_{k' \rightarrow l} = ICL(\mathbf{z}^*, K) - ICL(\mathbf{z}, K).$$

³Hereafter, the “*” notation refers to the statistics *after* switching/merging.

The only statistics not simplifying, are those involving k' and l , hence the equation above can be read as follows

$$\begin{aligned}
\Delta_{k' \rightarrow l} &:= \log \left(\frac{\Gamma(|\mathcal{A}_{k'}| - 1 + \alpha) \Gamma(|\mathcal{A}_l| + 1 + \alpha)}{\Gamma(|\mathcal{A}_{k'}| + \alpha) \Gamma(|\mathcal{A}_l| + \alpha)} \right) \\
&+ \sum_{g \leq K} \sum_{u \leq U} \log(L_{k'gu}^*) + \sum_{g \leq K} \sum_{u \leq U} \log(L_{lgu}^*) \\
&+ \sum_{k \leq K} \sum_{u \leq U} \log(L_{kk'u}^*) + \sum_{k \leq K} \sum_{u \leq U} \log(L_{klu}^*) \\
&- \sum_u (\log(L_{k'k'u}^*) + \log(L_{k'lu}^*) + \log(L_{lk'u}^*) + \log(L_{llu}^*)) \\
&- \sum_{g \leq K} \sum_{u \leq U} \log(L_{k'gu}) - \sum_{g \leq K} \sum_{u \leq U} \log(L_{lgu}) \\
&- \sum_{k \leq K} \sum_{u \leq U} \log(L_{kk'u}) - \sum_{k \leq K} \sum_{u \leq U} \log(L_{klu}) \\
&+ \sum_u (\log(L_{k'k'u}) + \log(L_{k'lu}) + \log(L_{lk'u}) + \log(L_{llu})),
\end{aligned} \tag{22}$$

where L_{kgu} is the term inside the product on the right hand side of equation (19) and \mathbf{z}^* and L_{kdu}^* refer to new configuration where the node i in in \mathcal{A}_l .

When merging clusters $\mathcal{A}_{k'}$ and \mathcal{A}_l into the cluster \mathcal{A}_l , the change in the ICL can be expressed as follows:

$$\begin{aligned}
\Delta_{k' \rightarrow l} &:= ICL(\mathbf{z}^*, K - 1) - ICL(\mathbf{z}, K) = \\
&= \log \left(\frac{p(\mathbf{z}^* | K - 1)}{p(\mathbf{z} | K)} \right) + \\
&+ \sum_{g \leq K} \sum_{u \leq U} (\log(L_{lgu}^*) + \log(L_{klu}^*)) - \sum_u \log(L_{llu}^*) \\
&- \sum_{g \leq K} \sum_{u \leq U} \log(L_{k'gu}) - \sum_{g \leq K} \sum_{u \leq U} \log(L_{lgu}) \\
&- \sum_{k \leq K} \sum_{u \leq U} \log(L_{kk'u}) - \sum_{k \leq K} \sum_{u \leq U} \log(L_{klu}) \\
&+ \sum_u (\log(L_{k'k'u}) + \log(L_{k'lu}) + \log(L_{lk'u}) + \log(L_{llu})).
\end{aligned} \tag{23}$$

When working with model **B**, we need to initialize D_{max} and \mathbf{y} . Then a shuffled sequence of time intervals I_1, \dots, I_U is considered and each interval is swapped to the time cluster leading to the highest increase in the ICL (**GE** for time intervals). When no further increase in the ICL is possible, we look for possible merges between time clusters in the attempt to increase the ICL (**GM** for time intervals). Formulas to directly assess the increase in the ICL can be obtained, similar to those for nodes swaps and merges. In case of model **B**, different strategies are possible to optimize the ICL:

1. **GE** + **GM** for nodes at first and then for times (we will call this strategy **TN**, henceforth).
2. **GE** + **GM** for time intervals at first and then for nodes (**NT** strategy).

- 215 3. An hybrid strategy, involving alternate switching of nodes and time intervals
(**M** strategy).

We will provide details about the chosen strategy case by case in the following.

5. Experiments

In this section, experiments on both synthetic and real data are provided.
220 All running times are measured on a twelve cores Intel Xeon server with 92 GB
of main memory running a GNU Linux operating system, the greedy algorithm
described in Section 4.4 being implemented in C++. A Euclidean hierarchical
clustering algorithm was used to initialize the labels and K_{max} was set to $N/2$.

In the following, we call TSBM the temporal SBM we propose and we refer
225 to the optimization algorithm described in the previous section as greedy ICL.

5.1. Simulated Data

5.1.1. First Scenario

We start by investigating how the proposed approach can be used to efficiently
estimate the vector \mathbf{z} of labels in situations where the standard SBM fails. Thus,
we simulate interactions between 50 (N) nodes, grouped in two hidden clusters
 \mathcal{A}_1 and \mathcal{A}_2 , over 100 (U) time intervals of unitary length. The generative model
considered for the simulations depends on two time clusters \mathcal{C}_1 and \mathcal{C}_2 containing
a certain number of time intervals I_1, \dots, I_U . If I_u is in \mathcal{C}_1 then $Y_{ij}^{I_u}$ is drawn
from a Poisson distribution $\mathcal{P}(P_{z_i z_j})$. Otherwise, $Y_{ij}^{I_u}$ is drawn from a Poisson
distribution $\mathcal{P}(Q_{z_i z_j})$. The matrices P and Q are given by

$$P = \begin{pmatrix} \psi & 1 \\ 1 & \psi \end{pmatrix} \quad \text{and} \quad Q = \begin{pmatrix} 1 & \psi \\ \psi & 1 \end{pmatrix},$$

where ψ is a free parameter in $[1, \infty)$. When this parameter is equal to 1,
we are in a degenerate case and there is not any structure to detect: all the
nodes are placed in the same, unique cluster. The higher ψ , the stronger the
contrast between the interactions pattern inside and outside the cluster. In this
paragraph, ψ is set equal to 2 and the proportions of the clusters are set equal
($\omega = (1/2, 1/2)$). The number of time intervals assigned to each time cluster is
assumed to be equal to $U/2$. In the following, we consider

$$\begin{aligned} \mathcal{C}_1 &:= \{I_1, \dots, I_{25}\} \cup \{I_{51}, \dots, I_{75}\}, \\ \mathcal{C}_2 &:= \{I_{26}, \dots, I_{50}\} \cup \{I_{76}, \dots, I_{100}\}. \end{aligned}$$

This generative model defines two integrated intensity functions (IIFs), say $\Lambda_1(t)$
and $\Lambda_2(t)$. The former is the IIF of the Poisson processes counting interactions
230 between nodes sharing the same cluster, the latter is the IIF of the Poisson
processes counting interactions between vertices in different clusters. These IIFs
can be observed in Figure 1a.

A tensor Y , with dimensions $N \times N \times U$, is drawn. Its (i, j, u) component is
the sampled number of interactions from node i to node j over the time interval

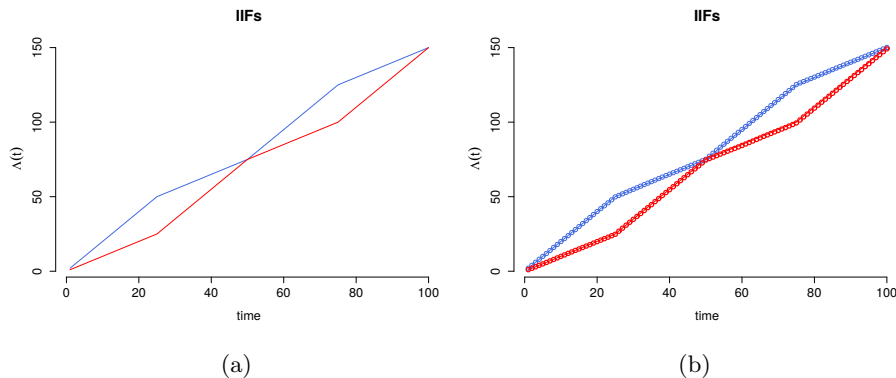


Figure 1: Real 1a and estimated 1b integrated intensity functions (IIFs) according to the considered generative model ($\psi = 2$). In blue we have $\Lambda_1(t)$, for $\psi = 4$, in red $\Lambda_2(t)$.

235 I_u . Moreover, sampled interactions are aggregated over the whole time horizon
to obtain an adjacency matrix. In other words, each tensor is integrated over
its third dimension. We compared the greedy ICL algorithm with the Gibbs
sampling approach introduced by Nouedoui and Latouche (2013). The former
was run on the tensor Y (providing estimates in 11.86 *seconds* on average) the
240 latter on the corresponding adjacency matrix. This experiment was repeated 50
times and estimates of random vector \mathbf{z} were provided at each iteration. Each
estimate $\hat{\mathbf{z}}$ is compared with the true \mathbf{z} and an adjusted rand index (ARI Rand,
1971) is computed. This index takes values between zero and one, where one
corresponds to the perfect clustering (up to label switching).

245 **Remark 5.** *the true structure is always recovered by the TSBM: 50 unitary
values of the ARI are obtained. Conversely, the standard SBM never succeeds in
recovering any hidden structures present in the data (50 null ARIs are obtained).
This can easily be explained since the time clusters have opposite interaction
patterns, making them hard to uncover when aggregating over time.*

250 Relying on an efficient estimate of \mathbf{z} , the two integrated intensity functions
can be estimated through the estimator in equation (15). Results can be observed
in Figure 1b, where the estimated functions (coloured dots) overlap the real
functions 1a.

Over fitting. We now illustrate how the model discussed so far fails in recovering
the true vector \mathbf{z} when the number of time intervals (and hence of free parameters)
grows. We consider the same generative model of the previous paragraph, with
a lower ψ :

$$P = \begin{pmatrix} 1.4 & 1 \\ 1 & 1.4 \end{pmatrix} \quad \text{and} \quad Q = \begin{pmatrix} 1 & 1.4 \\ 1.4 & 1 \end{pmatrix}.$$

Despite the lower contrast (from 2 to 1.4 in P and Q), with $U = 100$ and time
sub-intervals of unitary length, the TSBM model still always recovers the true

vector \mathbf{z} . Now we consider a finer partition of $[0, 100]$ by setting $U = 1000$ and $\Delta_u = 0.1$ as well as scaling the intensity matrices as follows

$$\tilde{P} := \begin{pmatrix} 0.14 & 0.1 \\ 0.1 & 0.14 \end{pmatrix} \quad \text{and} \quad \tilde{Q} = \begin{pmatrix} 0.1 & 0.14 \\ 0.14 & 0.1 \end{pmatrix}.$$

Moreover, we set

$$\mathcal{C}_1 := \{I_1, \dots, I_{250}\} \cup \{I_{501}, \dots, I_{750}\}$$

and \mathcal{C}_2 is the complement of \mathcal{C}_1 , as previously. Finally, we sampled 50 dynamic
 255 graphs over the interval $[0, 100]$ from the corresponding generative model. Thus, each graph is characterized by a sampled tensor Y .

Unfortunately, the model is not robust to such changes. Indeed, when running the greedy ICL algorithm on each sampled tensor Y , the algorithm does not see any community structure and all nodes are placed in the same cluster. This
 260 leads to a null ARI, for each estimation. As mentioned in paragraph 4.4, the ICL penalizes the number of parameters and since the tensor π has dimension $K \times K \times U$, for a fixed K , when moving from the larger decomposition ($U = 100$) to the finer one ($U = 1000$), the number of free parameters in the model is approximately⁴ multiplied by 10. The increase we observe in the likelihood,
 265 when increasing the number of clusters of nodes from $K = 1$ to $K = 2$, is not sufficient to compensate the penalty due to the high number of parameters and hence the ICL decreases. Therefore, the maximum is taken for $K = 1$ and a single cluster is detected.

Model **B** allows to tackle this issue. When allowing the integrated intensity
 270 functions $\Lambda_1(t)$ and $\Lambda_2(t)$ to grow at the same rate on each interval I_u belonging to the same time cluster \mathcal{C}_d , we basically reduce the third dimension of the tensor π from U to D .

The greedy ICL algorithm for Model **B** was run on each sampled tensor Y , providing estimates of \mathbf{z} and \mathbf{y} in 2.38 *minutes*, on average. A hierarchical
 275 clustering algorithm was used to initialize the time labels \mathbf{y} , and the initial number of time clusters was set to $D_{max} = \sqrt{U}$. In an attempt to avoid convergence to local maxima, ten estimates are built for each tensor and the estimate leading to the best ICL is finally retained. The adjusted rand index is used to evaluate the clustering, as previously, and the results are presented as box
 280 plots in Figure 2. Note that the results were obtained through the optimization strategy **TN**. The other two strategies described in section 4.4, namely the **NT** strategy and the **M** strategy, led to similar results in terms of final ICL and ARIs.

5.1.2. Second Scenario

285 Since the node clusters are fixed over time, the TSBM model can be seen as an alternative to a standard SBM to estimate the label vector \mathbf{z} . The previous

⁴The dimension of the vector ω does not change.

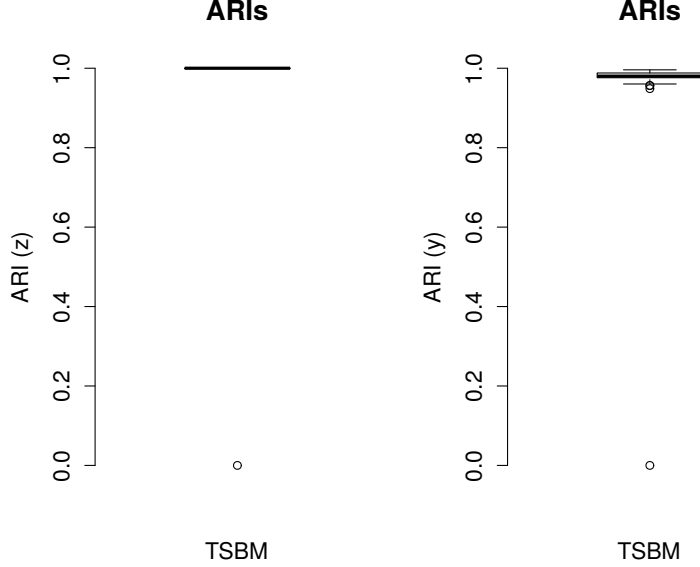


Figure 2: Box plots for both clusterings of nodes and time intervals: 50 dynamic graphs were sampled according to the considered generative model, estimates of \mathbf{z} and \mathbf{y} are provided by the greedy ICL (model B).

scenario shows that the TSBM can recover the true vector \mathbf{z} in situations where the SBM fails. In this paragraph we show how the TSBM and the SBM can sometimes have similar performances.

We considered dynamic graphs with 50 (N) nodes and 50 (U) time intervals

$$I_1, \dots, I_{50}.$$

These time intervals are grouped in two time clusters \mathcal{C}_1 and \mathcal{C}_2 , the former containing the first 25 time intervals, the latter the last 25 time intervals. If I_u is in \mathcal{C}_1 then $Y_{ij}^{I_u}$ is drawn from a Poisson distribution $\mathcal{P}(P_{z_i z_j})$. Otherwise, $Y_{ij}^{I_u}$ is drawn from a Poisson distribution $\mathcal{P}(2P_{z_i z_j})$. The P matrix is given by

$$P = \begin{pmatrix} \psi & 2 \\ 2 & \psi \end{pmatrix}$$

and ψ is a free parameter in $[2, +\infty)$. Hence, we have two different integrated intensity functions, say $\Lambda_1(t)$ and $\Lambda_2(t)$ with the same roles as in the previous section. These two functions are plotted in Figure 3a, for a value of $\psi = 4$.

We investigated six values for the parameter ψ

$$\{2.1, 2.2, 2.3, 2.4, 2.5, 2.6\}.$$

For each value of ψ , we sampled 50 tensors Y , of dimension $(50 \times 50 \times 50)$, according to the generative model considered. Interactions are aggregated over

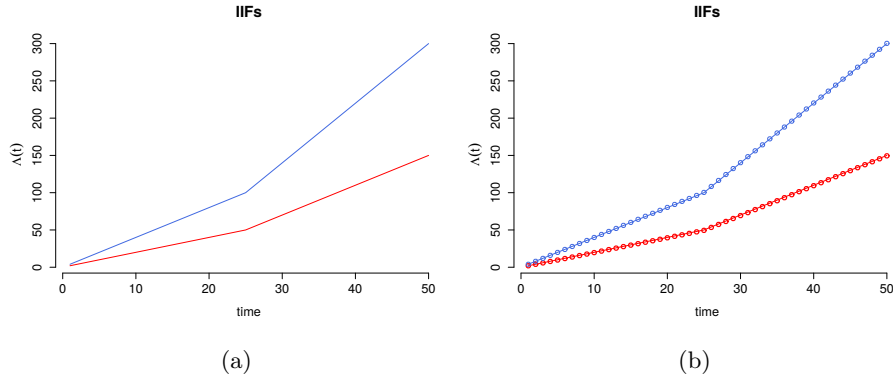


Figure 3: Real 3a and estimated 3b integrated intensity functions (IIFs) according to the considered generative model. In blue we have $\Lambda_1(t)$, for $\psi = 4$, in red $\Lambda_2(t)$.

295 the time interval $[0, 50]$ to obtain adjacency matrices. We ran the greedy ICL
 algorithm on each tensor and the Gibbs sampling (SBM) algorithm on each
 adjacency matrix. For the greedy ICL algorithm, estimates of vector \mathbf{z} were
 obtained in a mean running time of 5.52 *seconds*. As previously, to avoid
 convergence to local maxima, ten different estimates are built for each tensor,
 300 the one leading to the highest ICL being retained. The results are presented
 as box plots in Figure 4. Although the SBM leads to slightly better clustering

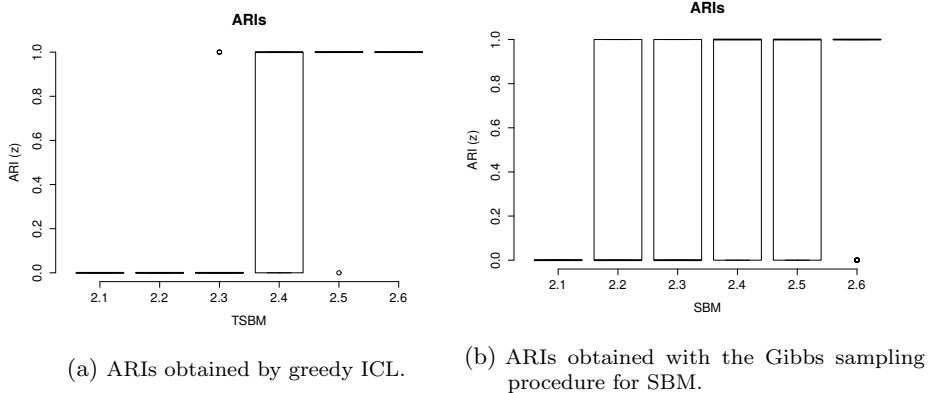


Figure 4: Box plots of ARIs for different levels of contrast (ψ). We compare the proposed model with a standard SBM.

results for small values of ψ (2.2, 2.3) and the TSBM for higher values of ψ (2.5, 2.6), we observe that the two models have quite similar performances (in terms of accuracy) in this scenario.

To provide some intuitions about the scalability (see next paragraph) of the proposed approach we repeated the previous experiment by setting $K = 3$

clusters, corresponding to the following connectivity matrix:

$$P = \begin{pmatrix} \psi & 2 & 2 \\ 2 & \psi & 2 \\ 2 & 2 & \psi \end{pmatrix}.$$

305 The assignment of the time intervals to the time clusters is unchanged as well as the connectivity pattern on each time cluster are unchanged. The contrast parameter ψ takes values in the set $\{2, 2.5, 2.10, \dots, 2.8\}$ and 50 dynamic graphs were sampled, according to the described settings, for each value of ψ . We ran the TSBM on each dynamic graph obtaining 50 estimates of the labels vector \mathbf{z}
 310 (one for each ψ) and box and whiskers plots for each group of ARIs can be seen in Figure 5. By comparing this figure with Figure 4a, we can see that the model

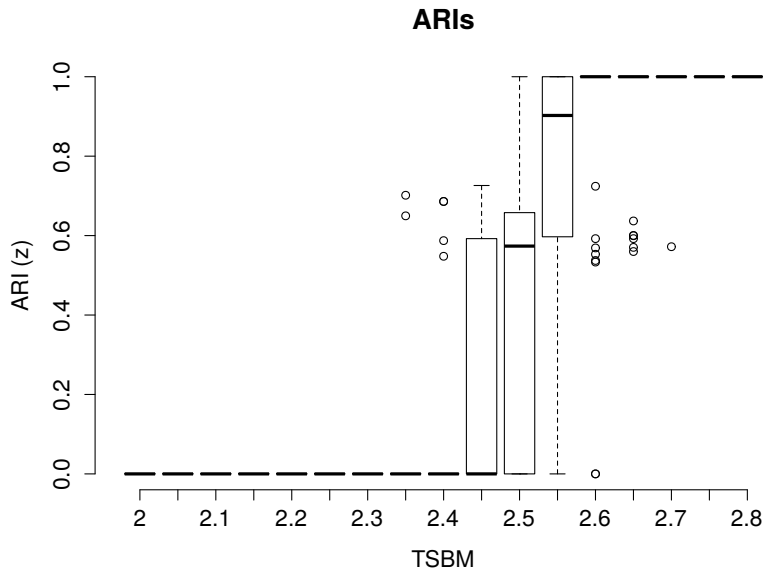


Figure 5: Box plots of ARIs for different levels of contrast (ψ). Data have been sampled by non-homogeneous Poisson processes counting interactions in a dynamic graph whose nodes are grouped in three clusters and interactivity patterns vary across two time clusters.

needs a slight higher contrast to fully recover the true structure. Actually, when increasing the number of clusters without increasing the number of nodes, the size of each cluster decreases (on average) and since the estimator of \mathbf{z} we are
 315 using is related to the ML estimator, we can imagine a slower convergence to the true value of \mathbf{z} .

5.1.3. Scalability

A full scalability analysis of the proposed algorithm as well as the convergence properties of the proposed estimators are outside the scope of this paper.

320 Nonetheless, in appendix we provide details about the computational complexity of the greedy-ICL algorithm. Future works could certainly be devoted to improve both the algorithm efficiency and scalability through the use of more sophisticated data structures.

5.2. Real data

325 The dataset used in this section was collected during the **ACM Hypertext** conference held in Turin, June 29th - July 1st 2009. We focus on the first conference day (24 hours) and consider a dynamic network with 113 (N) nodes (conference attendees) and 96 (U) time intervals (the consecutive quarter-hours in the period: 8am of June 29th - 7.59am of June 30th). The network edges are
 330 the proximity face to face interactions between the conference attendees. An interaction is monitored when two attendees are face to face, nearer than 1.5 meters for a time period of at least 20 seconds⁵. The data set we considered consists of several lines similar to the following one

<i>ID1</i>	<i>ID2</i>	<i>Time Interval (15m)</i>	<i>Number of interactions</i>
52	26	5	16

335 It means that conference attendees 52 and 26, between 9am and 9.15am, have spoken for $16 \times 20s \approx 5m30s$.

We set $K_{max} = 20$ and the vector \mathbf{z} was initialized randomly: each node was assigned to a cluster following a multinomial distribution. The greedy algorithm was run ten times on the considered dataset, each time with a different
 340 initialization and estimates of \mathbf{z} and K were provided in 13.81 *seconds*, on average. The final values of the ICL can be observed as box plots in Figure 6 .

The estimates associated to the highest ICL correspond to 5 node clusters. In Figure 7, we focus on the cluster \mathcal{A}_4 , containing 48 nodes. In Figure 7a we plotted the time cumulated interactions inside the cluster. As it can be seen the connectivity pattern for this cluster is very representative of the entire graph: between 13pm and 14pm and 18pm and 19.30pm there are significant increases in the interactions intensity. The estimated integrated intensity function (IIF) for interactions inside this cluster can be observed in Figure 7b. The function has a higher slope on those time intervals where attendees in the cluster are
 345 more likely to have interactions. The vertical red lines delimit two important times of social gathering⁶:

- 13.00-15.00 - lunch break.
- 18.00-19.00 - wine and cheese reception.

⁵More informations about the way the data were collected can be found in Isella et al. (2011) or visiting the website <http://www.sociopatterns.org/datasets/hypertext-2009-dynamic-contact-network/>.

⁶More informations at <http://www.ht2009.org/program.php>.

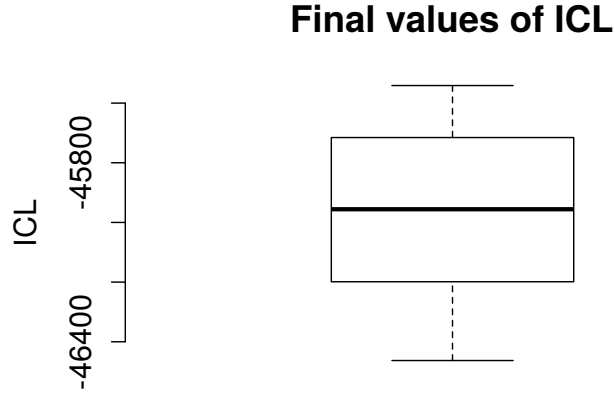
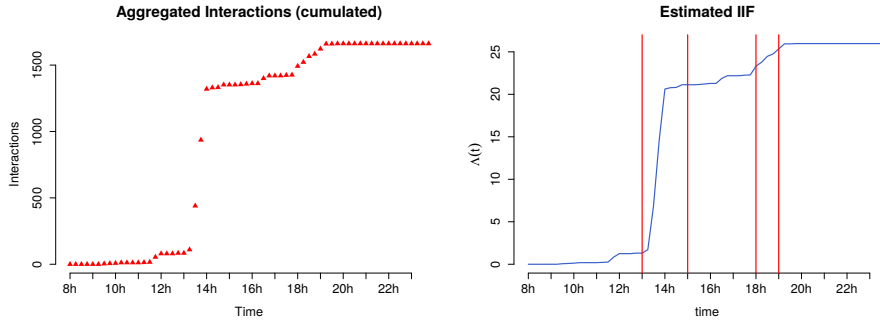


Figure 6: Box plot of the ten final values of the ICL produced by the greedy ICL algorithm for different initializations.

We conclude this section by illustrating how Model **B** can be used to assign
 355 time intervals on which interactions have similar intensity to the same time
 cluster. We run the greedy ICL algorithm for Model **B** on the dataset by using
 the optimization strategy **M** described at the end of Section 4.4 (other strategies
 lead in this case to similar results) and D_{max} was set equal to 20. The time
 clustering provided by the greedy ICL algorithm can be observed in Figure 8.
 360 On the left hand side, the aggregated interactions for each quarter-hour during
 the first day are reported. On the right hand side, interactions taking place into
 those time intervals assigned to the same time cluster have the same form/color.
 Two important things should be noticed:

1. The obtained clustering seems meaningful: the three time intervals with
 365 the highest interactions level are placed in the same cluster (blue), apart
 from all the others. More in general, each cluster is associated to a certain
 intensity level, so time intervals in the same cluster, not necessarily adjacent,
 share the same global interactivity pattern.
2. There are not constraints on the number of abruptly changes connected
 370 with these five time clusters. In other words, time clusters do not need to
 be adjacent and this is the real difference between the approach considered
 in this paper (time clustering) and a pure segmentation one.



(a) Cumulated aggregated connections inside cluster \mathcal{A}_4 . (b) Estimated IIF for interactions inside cluster \mathcal{A}_4 .

Figure 7: in Figure 7a, cumulated aggregated connections for each time interval for cluster \mathcal{A}_4 . In Figure 7b the estimated IIF for interactions inside cluster \mathcal{A}_4 . Vertical red lines delimit the lunch break and the wine and cheese reception.

6. Conclusion

We proposed a non-stationary extension of the stochastic block model (SBM) allowing us to cluster nodes of a network in situations where the classical SBM fails. The approach we chose consists in partitioning the time interval over which interactions are studied into sub-intervals of fixed length. Those intervals provide aggregated interaction counts that are increments of non homogeneous Poisson processes (NHPPs). In a SBM inspired perspective, nodes are clustered in such a way that aggregated interaction counts are homogeneous over clusters. We derived an exact integrated classification likelihood (ICL) for such a model and proposed to maximize it through a greedy search strategy. Finally, a non parametric maximum likelihood estimator was developed to estimate the integrated intensity functions of the NHPPs counting interactions between nodes. The experiments we carried out on artificial and real world networks highlight the capacity of the model to capture non-stationary structures in dynamic graphs.

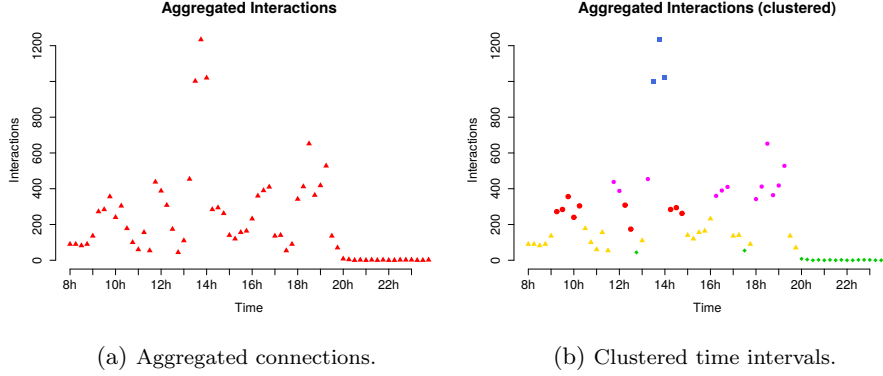


Figure 8: in Figure 8a, aggregated connections for each time interval for the whole network. In Figure 8b interactions of the same form/color take place on time intervals assigned to the same cluster (model **B**).

Appendix A. Computational complexity

In this section we provide details about the computational complexity of the main model presented in this paper, namely the model **A**. Assuming that the gamma function can be computed in constant time (see Press et al., 2007), we focus on the three statistics appearing in equation (9), namely

1. $S_{kgu} := \sum_{z_i=k} \sum_{z_j=g} Y_{ij}^{I_u}$,
2. $P_{kgu} := \prod_{z_i=k} \prod_{z_j=g} Y_{ij}^{I_u}!$,
3. $R_{kg} := |\mathcal{A}_k| |\mathcal{A}_g|$.

The whole computation task consists in evaluating the increase in ICL induced by nodes exchanges and merges. Those computations involves the tree quantities listed above. The tensor $\{S_{kgu}\}_{k,g \leq K, u \leq U}$ is stored in a three dimensional array, never resized, occupying a $O(K_{max}^2 U)$ memory space. Hence, at any time during the algorithm its elements can be accessed and modified in constant time. The tensor $\{P_{kgu}\}_{k,g \leq K, u \leq U}$ is handled similarly and clusters sizes (we recall that $|\mathcal{A}_k|$ corresponds to the size of cluster \mathcal{A}_k) are also stored in arrays. In order to evaluate the ICL changes, induced by an operation, we need to maintain aggregated interaction counts for each node: for a node i we have, e.g.

$$S_{igu} := \sum_{z_j=g} Y_{ij}^{I_u},$$

the number of interactions from node i to cluster \mathcal{A}_g inside the time interval I_u . Similarly

$$S'_{igu} := \sum_{z_j=g} Y_{ji}^{I_u}$$

denotes the number of interactions from cluster \mathcal{A}_g to node i inside the time interval I_u . Other related quantities are considered. These structures occupy a memory space of $O(N^2 U)$.

Exchanges. In order to evaluate the ICL increase induced by the switch of a node (say i) from cluster $\mathcal{A}_{k'}$ to cluster \mathcal{A}_l , we perform the following operations:

- 400 • $S_{k'gu}$ (respectively $S_{gk'u}$) is reduced by S_{igu} (S'_{igu}) and S_{lgu} (S_{glu}) is increased by the same amount;
- $P_{k'gu}$ (respectively $P_{g'ku}$) is reduced by P_{igu} (P'_{igu}) and P_{lgu} (P_{glu}) is increased by the same amount;
- $\mathcal{A}_{k'}$ (\mathcal{A}_l) is reduced (increased) by one.

405 Although these operations are in constant time, they are involved in a sum with (KU) elements (this can be seen in equation (22)), so that the total cost of the test is $O(KU)$. Since node i can be switched to $K - 1$ remaining clusters and the graph has N nodes, the cost of a *full* exchange routine is $O(NK^2U)$.

Remark 6. *When a node is actually switched from its cluster to another one,*
410 *all data structures are updated but the update cost is dominated by the cost of the testing phase described above.*

Notice that we have evaluated the total cost of one full exchange routine, i.e., in the case where all nodes are considered once. Reductions in the number of clusters (very likely to be induced by exchanges in case K_{max} is high) are not
415 taken into account.

Merges. The entire merge routine, consisting in a test phase and an actual merge, has a computational cost that is dominated by the cost of exchanges. Consider a cluster $\mathcal{A}_{k'}$. We first look for the cluster (say \mathcal{A}_l) leading to the best merge (highest increase in the ICL) with $\mathcal{A}_{k'}$. This operation has a cost of
420 $O(K^2U)$: for each \mathcal{A}_l the evaluation of the increase in ICL has a cost of $O(KU)$ (see equation (23)) and l can take $K - 1$ possible values. Since we look for the best merge for all $k' \in \{1, \dots, K\}$ the computational cost for a merge of two nodes clusters is $O(K^3U)$, where we recall that $D \leq N$.

Total cost. The worst case complexity for one iteration of the algorithm, with
425 each node considered once, is $O(NK^2U)$. However, it is difficult to evaluate the actual complexity of the whole algorithm for two reasons. Firstly, we have no way to estimate the number of exchanges needed in the exchange phase. Secondly, nodes exchanges are very likely to reduce the number of clusters, especially at the beginning of the algorithm, when K_{max} is relatively high. Thus the individual
430 cost of an exchange reduces very quickly leading to a vast overestimation of its cost using the proposed bounds. A detailed evaluation of the behaviour of the proposed algorithm, although outside the scope of the this paper, would be necessary to assess its use on large data sets.

References

- 435 Biernacki, C., Celeux, G., Govaert, G., 2000. Assessing a mixture model for clustering with the integrated completed likelihood. *Pattern Analysis and Machine Intelligence*, IEEE Transactions on 22 (7), 719–725.

- Blondel, V. D., loup Guillaume, J., Lambiotte, R., Lefebvre, E., 2008. Fast unfolding of communities in large networks.
- 440 Côme, E., Latouche, P., 2015. Model selection and clustering in stochastic block models based on the exact integrated complete data likelihood. *Statistical Modelling* 15 (6), 564–589.
- Corneli, M., Latouche, P., Rossi, F., Aug. 2015. Modelling time evolving interactions in networks through a non stationary extension of stochastic block models. In: Pei, J., Silvestri, F., Tang, J. (Eds.), *International Conference on Advances in Social Networks Analysis and Mining ASONAM 2015*. IEEE/ACM, ACM, Paris, France, pp. 1590–1591.
URL <https://hal.archives-ouvertes.fr/hal-01263540>
- 450 Dubois, C., Butts, C., Smyth, P., 2013. Stochastic blockmodelling of relational event dynamics. In: *International Conference on Artificial Intelligence and Statistics*. Vol. 31 of the *Journal of Machine Learning Research Proceedings*. pp. 238–246.
- Fortunato, S., 2010. Community detection in graphs. *Physics Reports* 486 (3-5), 75 – 174.
- 455 Goldenberg, A., Zheng, X., Fienberg, S. E., Airoldi, E. M., 2009. A survey of statistical network models. *Machine Learning* 2 (2), 129–133.
- Guigourès, R., Boullé, M., Rossi, F., 12 2012. A triclustering approach for time evolving graphs. In: *Co-clustering and Applications, IEEE 12th International Conference on Data Mining Workshops (ICDMW 2012)*. Brussels, Belgium, pp. 115–122.
460
- Guigourès, R., Boullé, M., Rossi, F., 2015. Discovering patterns in time-varying graphs: a triclustering approach. *Advances in Data Analysis and Classification*, 1–28.
URL <http://dx.doi.org/10.1007/s11634-015-0218-6>
- 465 Holland, P., Laskey, K., Leinhardt, S., 1983. Stochastic blockmodels: first steps. *Social Networks* 5, 109–137.
- Isella, L., Stehl, J., Barrat, A., Cattuto, C., Pinton, J., Van den Broeck, W., 2011. What’s in a crowd? analysis of face-to-face behavioral networks. *Journal of Theoretical Biology* 271 (1), 166–180.
- 470 Leemis, L. M., 1991. Nonparametric estimation of the cumulative intensity function for a nonhomogeneous poisson process. *Management Science* 37 (7), 886–900.
URL <http://www.jstor.org/stable/2632541>
- 475 Lorrain, F., White, H., 1971. Structural equivalence of individuals in social networks. *Journal of Mathematical Sociology* 1 (49-80).

- Matias, C., Rebafka, T., Villers, F., Dec. 2015. Estimation and clustering in a semiparametric Poisson process stochastic block model for longitudinal networks. ArXiv e-prints.
- Noack, A., Rotta, R., 2008. Multi-level algorithms for modularity clustering. CoRR abs/0812.4073.
 480 URL <http://arxiv.org/abs/0812.4073>
- Nouedoui, L., Latouche, P., 2013. Bayesian non parametric inference of discrete valued networks. In: 21-th European Symposium on Artificial Neural Networks, Computational Intelligence and Machine Learning (ESANN 2013). Bruges, Belgium, pp. 291–296.
 485
- Press, W. H., Teukolsky, S. A., Vetterling, W. T., Flannery, B. P., 2007. Numerical Recipes 3rd Edition: The Art of Scientific Computing, 3rd Edition. Cambridge University Press.
- Rand, W. M., 1971. Objective criteria for the evaluation of clustering methods. Journal of the American Statistical association 66 (336), 846–850.
 490
- Schaeffer, S. E., August 2007. Graph clustering. Computer Science Review 1 (1), 27–64.
- Wang, Y., Wong, G., 1987. Stochastic blockmodels for directed graphs. Journal of the American Statistical Association 82, 8–19.
- 495 Wasserman, S., Faust, K., 1994. Social network analysis: Methods and applications. Vol. 506. Cambridge University Press.
- White, H. C., Boorman, S., Breiger, R., 1976. Social structure from multiple networks: I. blockmodels of roles and positions. Am. J. of Sociology 81 (4), 730–80.
- 500 Wyse, J., Friel, N., Latouche, P., 2014. Inferring structure in bipartite networks using the latent block model and exact icl. arXiv preprint arXiv:1404.2911.
- Xing, E. P., Fu, W., Song, L., 06 2010. A state-space mixed membership blockmodel for dynamic network tomography. Ann. Appl. Stat. 4 (2), 535–566.
- Xu, K. S., Hero III, A. O., 2013. Dynamic stochastic blockmodels: Statistical models for time-evolving networks. In: Social Computing, Behavioral-Cultural Modeling and Prediction. Springer, pp. 201–210.
 505
- Yang, T., Chi, Y., Zhu, S., Gong, Y., Jin, R., 2011. Detecting communities and their evolutions in dynamic social networks a bayesian approach. Machine learning 82 (2), 157–189.